A statistical approach to identify fragmentation epoch from a single fragment surveillance radar observation

Marco Felice Montaruli
Politecnico di Milano, Department of Aerospace Science and Technology (DAER), Via G. La Masa 34, 20156, Milan, Italy
Pierluigi Di Lizia
Politecnico di Milano, Department of Aerospace Science and Technology (DAER), Via G. La Masa 34, 20156, Milan, Italy

Emiliano Cordelli
GMV@ESA, Space Debris Office (SDO), European Space Operations Centre (ESA/ESOC), Robert-Bosch-Str. 5, 64293 Darmstadt, Germany

Hélène Ma
RHEA System GmbH@ESA, Space Debris Office (SDO), European Space Operations Centre (ESA/ESOC), Robert-Bosch-Str. 5, 64293 Darmstadt, Germany

Jan Siminski
European Space Agency – European Space Operations Centre (ESA/ESOC), Robert-Bosch-Str. 5, 64293 Darmstadt, Germany

ABSTRACT

In the last decades, the growing in-orbit population of resident objects has become one of the main concerns for space agencies and institutions worldwide. In this context, fragmentations further contribute to increase the number of space debris and, operationally, it is fundamental to identify the event epoch as soon as possible, even when just a single fragment orbital state, resulting from an Initial Orbit Determination (IOD) process, is available.
This work illustrates the Fragmentation Epoch Detector (FRED) algorithm, which deals with the problem through a statistical approach, starting from a single fragment IOD result (expressed through mean state and covariance) and parent ephemeris (assumed as deterministic). The process populates the fragment ephemeris with a multivariate normal distribution and, for each couple sample-parent, the epochs of transit through the Minimum Orbital Intersection Distance (MOID) are first computed on a time window and then clustered in time. For each cluster, both the 3-dimensional MOID and the 3-dimensional relative distance distributions are derived (generally non-normal, the latter computed at the epoch of parent transit through the MOID), and their similarity is statistically assessed. At the end, the cluster featuring the best matching between the two distributions is considered as the optimal candidate, and the fragmentation epoch is returned from the time of parent transit through the MOID, in terms of mean and standard deviation.
FRED algorithm performance is assessed through a numerical analysis. An operational case which also embeds the IOD process starting from radar measurements is discussed as well.

1. INTRODUCTION

Space pollution has become a major concern for space agencies and institutions all around the world, since the number of man-made objects orbiting the Earth has dramatically increased. In 65 years of space activities, more than 6250 successful launches have taken place, which turned out in about 13630 objects placed in Earth orbit [1]. Among these, 8840 are still orbiting, but only 6200 are active. This hazard calls for the crucial adoption of countermeasures aiming

at reducing mission-related risks. Specific Space Surveillance and Tracking (SST) programs were started to build the expertise required to manage the challenges posed by the space traffic control problem.
Space debris are all artificial objects including fragments and elements thereof, in Earth orbit or re-entering the atmosphere, that are non functional [2]. Their presence may jeopardise the operative mission of active satellites, given that the possible impact with a space debris ranges from cumulative erosion of satellite surface, for debris smaller than 0.1 mm, to the possible satellite destruction, with the generation of thousands of additional pieces of debris and inevitable environmental drawbacks and possible cascade effects [3]. In this context, about 630 break-ups, explosions, collisions, or anomalous events resulting in fragmentation have been recorded from the beginning of the space activities, which have further contributed to increase the number of space debris [1]. Therefore, it is fundamental to predict the fragments cloud evolution, in order to assess possible collisions, and, for this reason, the event epoch shall be identified as soon as possible.
In [4] the event epoch is identified as the point of minimum distance of all the fragments with respect to the cloud centre of mass. Besides the accurate orbital ephemeris, this approach also assumes to own the physical information of each fragment, such as the mass and the cross sectional area. In [5] the break-up epoch is determined by detecting a convergence of fragments in the space of inclination and right ascension of the ascending node. In [6] a critical study is conducted to identify the best criterion to assess the event epoch from the fragments ephemerides and a sensitivity analysis on the cloud orbital position is also conducted. In [7] a process is proposed, which screens a catalogue of ephemerides and identifies those related to fragments, through the filters presented in [8]. After the filtering phase, the same criteria are applied combined with SGP4 propagation [9] [10] and, by comparing the algorithm outputs among all the fragments, the fragmentation epoch is assessed. The approaches in [6] and [7] remove the need of physical parameters (a part from the B*, that is the drag term used in SGP4 propagation by [7]), but many fragments ephemerides are still needed and used as a deterministic information.
The numerous accurate ephemerides availability of the space debris originated by the fragmentation event is a quite optimistic assumption, as, from an operational point of view, it could be necessary to estimate the fragmentation epoch just few hours after the event and very few ephemerides (even only one) could be available. In addition, when a fragments cloud is observed, the correlation of measurements to a single fragment is a very challenging task, and this further decreases the number of ephemerides which can be used in a reliable way. Next, such ephemerides could be inaccurate, because of the noise of the observation measurements and the uncertainty introduced by the Initial Orbit Determination (IOD) procedure, and their uncertainty cannot be neglected during the event characterisation. Nevertheless, a prompt knowledge of the fragmentation epoch would be fundamental to plan additional observations of the fragments cloud and also to refine the processing of the observation measurements, aiming at obtaining more and more accurate orbit determination results. This would lead to also refine the estimation of the fragmentation epoch and, so, a virtuous circle would be generated.
The aim of the present work is to provide an operational procedure to estimate the fragmentation epoch starting from the last available ephemeris of the parent object (assumed as a deterministic quantity) and a single fragment orbital state provided of uncertainty. The latter is considered as determined by a surveillance radar, which allows to run IOD from a single observation with no transit prediction. To accomplish this purpose, the FRagmentation Epoch Detector (FRED) algorithm, implementing a statistical approach, has been developed.

2. FRAGMENTATION EPOCH DETECTOR - FRED

Let's consider the fragmentation of a space object whose last available ephemeris $\boldsymbol{x}^p$ is dated to t_{eph}, and is considered as a deterministic information. The event has occurred at $t_0 > t_{eph}$ and the related alert has been notified at $t_a > t_0$. Some hours later, one fragment is detected by a surveillance radar at t_{obs} (with $t_{obs} > t_a$) and its orbital state $\left\{\boldsymbol{x}^{fg}, \boldsymbol{P}^{fg}\right\}$ is first determined, where the mean $\boldsymbol{x}^{fg}$ and covariance $\boldsymbol{P}^{fg}$ are directly derived from the IOD process.
If the orbit determination were very accurate and the physical parameters were well known, it would be theoretically possible to propagate both the fragment and the parent object in the time window $\left[t_{eph}, t_a\right]$ and search for the epoch of the minimum relative distance, which would correspond to the fragmentation epoch t_0. However, in real applications, both the measurements accuracy and the IOD process introduce an error in the reconstruction of the observed fragment state vector, and the above-mentioned method turns out to be unreliable. Fig. 1 represents the relative distance trend between the parent object and an observed fragment to which an IOD error of 1.85e-02 km in position and 4.99e-04 km/s in velocity is attributed (continuous black line). It can be observed that the epoch of minimum relative distance between the fragment mean state and the parent (dashed red line) is completely different from the correct fragmentation

epoch (dashed blue line), that is the epoch corresponding to the theoretical minimum relative distance (dashed black line). A further source of error is represented by the mismatching between the actual fragment trajectory and the propagation model used, due, for instance, to the fact that the actual physical parameters of the observed fragment are not known. For all these reasons, assessing the fragmentation epoch by just searching for the minimum relative distance between $\boldsymbol{x}^p$ and $\boldsymbol{x}^{fg}$ in the time window $\left[t_{eph}, t_a\right]$ is an unreliable methodology.

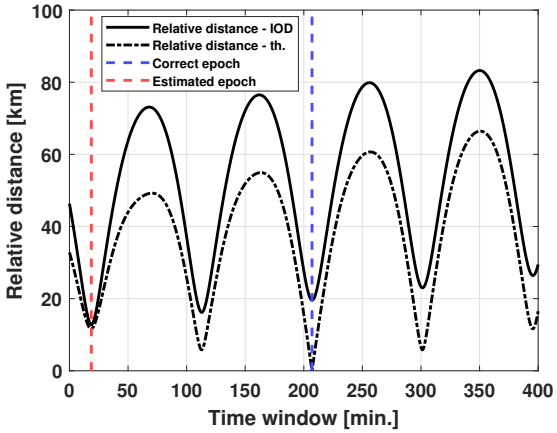

Fig. 1: Relative distance between the parent object and the mean state of one observed fragment. Their state vectors are propagated on a time window ranging from the last available ephemeris of the parent object to the event alert. The dashed black line shows the theoretical trend and the dashed blue line corresponds to the epoch of minimum value, that is the fragmentation epoch. On the contrary, the continuous black line shows the relative distance trend when an IOD error is attributed to the fragment mean state, and the dashed red line corresponds to the minimum value, that is the estimated fragmentation epoch. It is possible to see that the estimated fragmentation epoch is completely different from the correct value.

The considerations above imply that the orbit determination uncertainty cannot be a-priori neglected. For this reason FRED algorithm deals with the fragmentation epoch identification problem through a statistical approach, starting from a Monte Carlo distribution of the orbit determination result. Ideally, at the fragmentation epoch, both the Minimum Orbital Intersection Distance (MOID) [11] and the relative distance between the parent and the fragment are expected to be zero. Due to the considerations above, in practical cases neither MOID nor relative distance turn out to be null, but they should statistically match each other. Therefore, the correct fragmentation epoch is expected to feature a matching between the MOID and the relative distance distributions.
FRED algorithm is structured as follows.

1. In order to include the fragment state uncertainty in the event epoch identification, N_s samples $\boldsymbol{x}^s$ are generated from the orbital state $\left\{\boldsymbol{x}^{fg}, \boldsymbol{P}^{fg}\right\}$ according to a multinormal distribution [12].
2. The time window $\left[t_{eph}, t_a\right]$ is sampled with frequency $1/T^p$ (where T^p is the parent orbital period). This results in the epochs t_i, whose number is n_{orb}.
3. Both parent and fragment samples orbital states are propagated to each t_i.
4. For each t_i and for each j-th fragment sample, the epochs of transit through the MOID of both the parent and the fragment j-th sample are computed analytically, according to [11], and indicated as t_j^p and t_j^s. The parent and the j-th sample state vectors are propagated up to t_j^p and t_j^s respectively, resulting in the orbital states $\boldsymbol{x}^p(t_j^p)$ and $\boldsymbol{x}^s(t_j^s)$, and the analytical computations of t_j^p and t_j^s are updated. The epochs t_j^p and t_j^s are iteratively modified in this manner until, between two consecutive steps, they do not change anymore (according to a tolerance set equal to 1e-03 s).
   This iterative process results in $N_s \times n_{orb}$ couples of $\left(t_j^p,\, t_j^s\right)$ and $\left(\boldsymbol{x}^p(t_j^p),\, \boldsymbol{x}^s(t_j^s)\right)$. It is important to observe that

the difference between $\boldsymbol{p}^s(t_j^s)$ and $\boldsymbol{p}^p(t_j^p)$ (the $\boldsymbol{x}^s(t_j^s)$ and $\boldsymbol{x}^p(t_j^p)$ positions) allows to compute the MOID (usually described in a scalar way [11]) in a 3 dimensions: $\boldsymbol{m_j} = \boldsymbol{p}^s(t_j^s) - \boldsymbol{p}^p(t_j^p)$.

5. The fragment j-th sample state vector $\boldsymbol{x}^s(t_j^s)$ is propagated up to the epoch of parent transit through the MOID, resulting in $\boldsymbol{x}^s(t_j^p)$. It is worth to observe that the difference between the $\boldsymbol{p}^s(t_j^p)$ (the $\boldsymbol{x}^s(t_j^p)$ position) and $\boldsymbol{p}^p(t_j^p)$ provides the 3-dimensional relative distance between the j-th sample and the parent, at the epoch of parent transit through the MOID: $\boldsymbol{\rho_j} = \boldsymbol{p}^s(t_j^p) - \boldsymbol{p}^p(t_j^p)$. Fig. 2 provides a 2-dimensional sketch of the parent and fragment sample orbits, with the involved quantities.

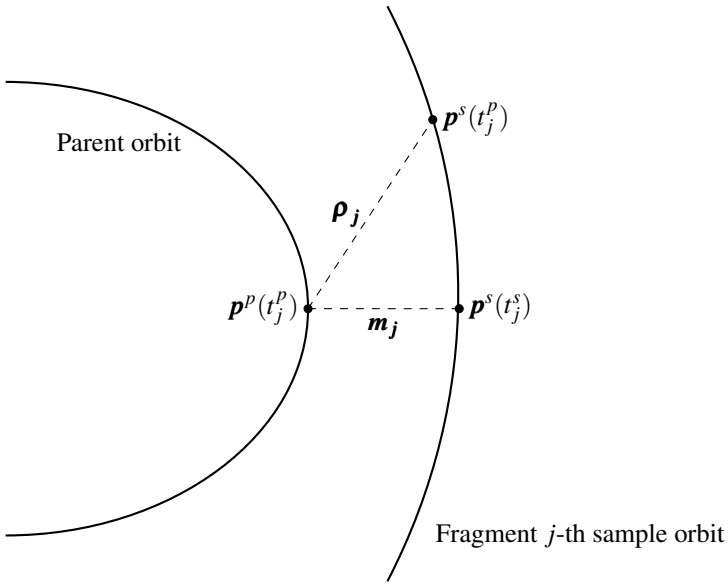

Fig. 2: Sketch of the parent and fragment sample orbits, with the quantities involved in FRED algorithm process.

6. To exclude unfeasible solutions, the $N_s \times n_{orb}$ couples enter a filtering phase, which is based on the epoch of parent transit through the MOID t_j^p. Being related to the deterministic part of the process (parent ephemeris), this is a much more reliable information than the time of the fragment j-th sample transit through the MOID t_j^s:
   (a) First, the couples for which t_j^p is not included in the boundaries $\left[t_{eph}, t_a\right]$ are removed from the data set.
   (b) Then, the couples computed from the state vectors propagated at epoch t_i and for which $t_j^p < (t_i - T^p/2)$ or $t_j^p > (t_i + T^p/2)$ are removed from the data set. This operation is done because the MOID data are computed for each periodicity. Thus, if t_j^p is computed from orbital states at t_i, it must belong to the i-th periodicity, that is the time difference $|t_i - t_j|$ shall be smaller than half of the orbital period T^p.

7. All the remaining n_{filter} epochs t_j^p are clustered according to a Density-Based Spatial Clustering of Applications with Noise (DBSCAN) [13]. From this operation, n_{orb} are expected to be identified. However, for those situations in which parent and fragment orbits are similar (especially in inclination and ascending node right ascension), multiple clusters are possibly identified for each i-th periodicity, as the epochs t_j^p change significantly from a j-th sample to another one. So, more generally, n_{cl} clusters are considered to be identified. Fig. 3a presents the obtained clusters, in the plane t_j^p (in Coordinated Universal Time, UTC) versus scalar MOID. It is worth to remark that the MOID values are equal from a periodicity to the other, as the graph is related to a keplerian scenario, in which, for a single parent j-th sample couple, the MOID does not change.

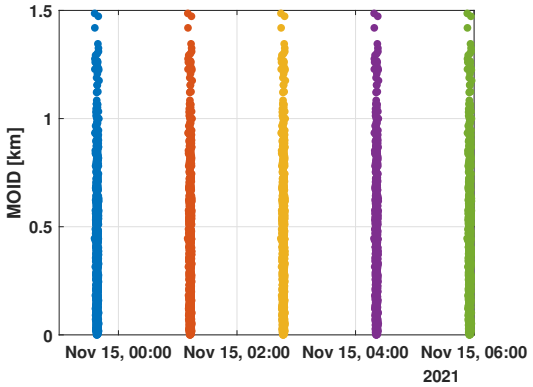

(a) Distribution of the t_j^p epochs in the time window of the analysis.

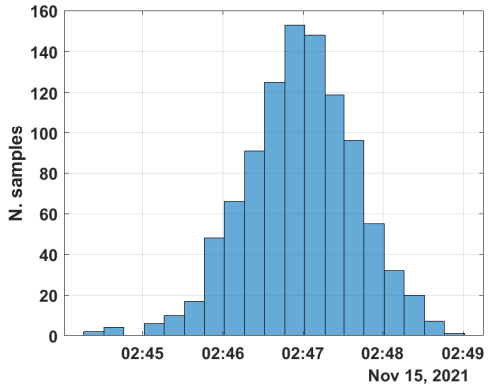

(b) Distribution of the t_j^p epochs for the cluster related to the correct solution.

Fig. 3: Result of the clustering phase. The epochs are reported in UTC.

8. For each n-th cluster, the candidate fragmentation epoch t_n^{fg} can be computed (in terms of mean and standard deviation) from the distribution of the epoch of parent transit through the MOID, which is indicated as F, and which is represented in Fig. 3b (for the correct cluster). In addition, $\boldsymbol{M}$ and $\boldsymbol{P}$ distributions (grouping the $\boldsymbol{m_j}$ and $\boldsymbol{\rho_j}$ respectively) are associated to each cluster. Fig. 4 shows the two distributions in Earth-Central-Inertial (ECI) reference frame, both for the correct candidate and for a not-correct one. It is possible to observe that the 3-dimensional MOID distribution $\boldsymbol{M}$ is much more concentrated than the relative distance one $\boldsymbol{P}$. This is due to the fact that, from sample to sample, the change in t_j^p causes a remarkable modification in the relative distance $\boldsymbol{\rho_j}$ (as it is time-dependent), but not in the MOID $\boldsymbol{m_j}$, whose variation only depends on the geometrical difference between the parent and the j-th sample orbits.

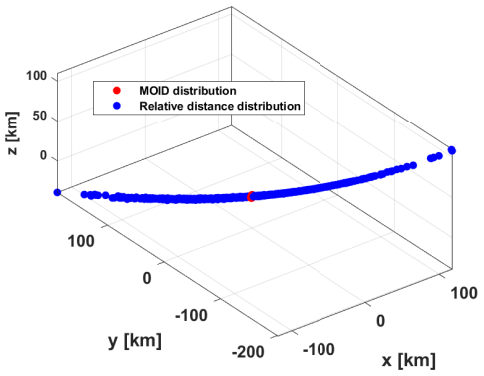

(a) Cluster related to the correct epoch.

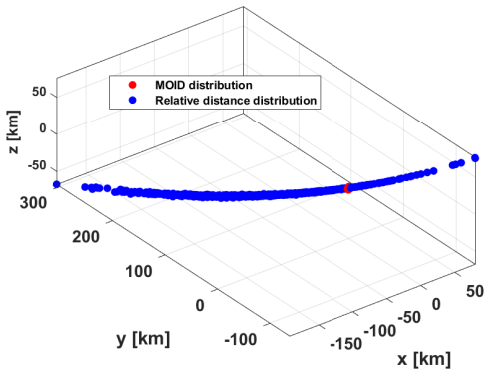

(b) Cluster related to a wrong epoch.

Fig. 4: $\boldsymbol{M}$ and $\boldsymbol{P}$ distributions in ECI reference frame, for the correct cluster and a not-correct one.

9. Afterwards, for each cluster:

   (a) All the $\boldsymbol{m_j}$ and $\boldsymbol{\rho_j}$ are rotated in the Modified Equidistant Cylindrical (EQCM) reference frame [14]. This operation results in MOID and relative distance distributions like in Fig. 5. The MOID distribution $\boldsymbol{M}$ is almost 2-dimensional, as, in all the $\boldsymbol{m_j}$, the y-component, expressing the along orbit curvature relative distance, is negligible for the MOID.

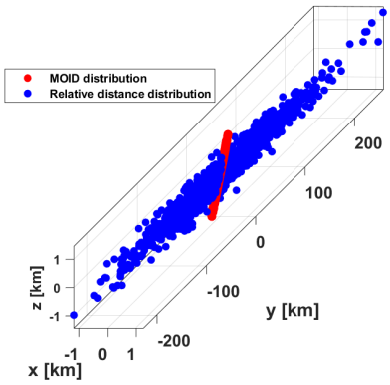

(a) Cluster related to the correct epoch.

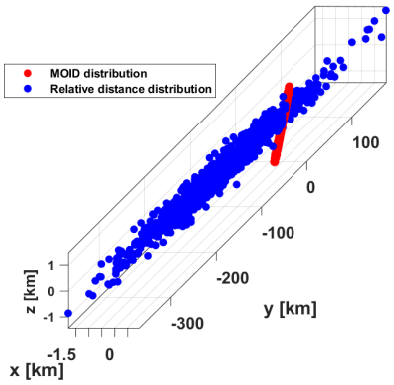

(b) Cluster related to a wrong epoch.

Fig. 5: ***M*** and ***P*** distributions in EQCM reference frame, for the correct cluster and a not-correct one.

(b) To be as generic and agnostic as possible regarding the distributions characteristics, the Earth Mover's Distance (EMD) [15] is selected to compare ***M*** and ***P*** for each cluster, as it is suitable for the no-Gaussian case as well. The implementation from [16] is used, and a metrics based on the euclidean distance weighted on the distribution variance is chosen to better account for its shape and elongation.

10. Repeating the operations above for each cluster results in Fig. 6, which shows the statistical distance in function of the F distribution mean. Finally, the cluster featuring the minimum statistical distance between the ***M*** and ***P*** distributions is selected, and the fragmentation epoch is returned from the related distribution F, in terms of mean and standard deviation.

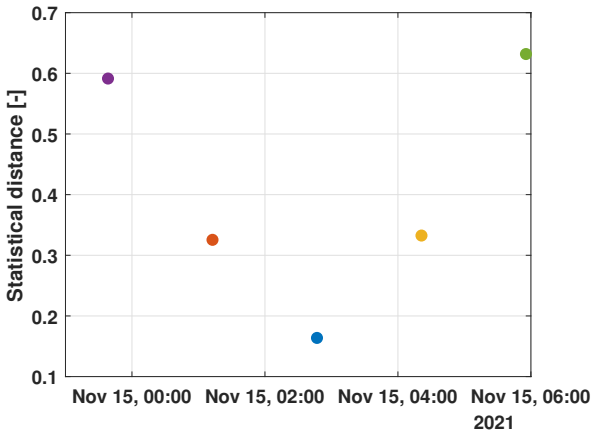

Fig. 6: EMD statistical distance computed for each cluster.

As mentioned above, this process provides a pattern to derive the fragmentation epoch (in terms of mean and standard deviation) through a statistical approach, starting from the last available parent ephemeris and the fragment IOD result. However, there are two theoretical sources of failure:

- The MOID computation turns out to be unstable when the the orbital planes of the fragment and parent orbits are very close each other (that is, they have similar inclination and right ascension of the ascending node). In this case, the slight change in the fragment orbit, occurring from sample to sample, can cause a remarkable variation in the MOID data computation. As result, for the correct candidate, F distribution does not cluster around the actual fragmentation epoch, but around an epoch distant up to tens of minutes.

- The relative distance distribution $\boldsymbol{P}$ does not change from a cluster to the other when the fragment and parent orbital shapes are very close each other (that is, they have similar semi-major axis and eccentricity). This makes their orbital periods similar as well and, for a j-th sample, from a i-th periodicity to the following one, the relative distance $\boldsymbol{\rho}_j$ does not change significantly. As result, it is not straightforward to recognise the correct cluster from the metrics described above, and the wrong fragmentation epoch is possibly returned by the process.

Sec. 3 assesses FRED performances and a more in-depth discussion on the failure situations is proposed.

3. NUMERICAL SIMULATIONS

A numerical simulation is here conducted to test the algorithm described in Sec. 2. The fragmentation scenario is the one which involved the Russian satellite COSMOS 1408 during the kinetic anti-satellite (ASAT) test which occurred around 02:47 UTC of November 15th, 2021 [17]. The ASAT test took place when the satellite was flying over the north-west Russia and the sensors of the European Space Surveillance and Tracking consortium [18] observed fragments generated by such an event.
The data set to test FRED algorithm is generated as follows:

1. The last available COSMOS 1408 ephemeris before the event are retrieved from the last TLE (Two-Line Elements) available on Spacetrack, which are dated to 00:55 UTC of November 15th [19]. To make the analysis time window more symmetrical with respect to the break-up event, they are propagated one orbital period back to the 23:20 UTC of November 14th, and the orbital state at this epoch is considered as $\boldsymbol{x_p}$.

2. The state vector $\boldsymbol{x_p}$ is propagated up to 02:47:00 UTC of November 15th. The fragmentation event is modelled as a series of impulses applied to the satellite orbital state at 02:47:00 UTC. These impulses are retrieved from the NASA standard break-up model [20]. A data set of 231 fragments is generated by this way, and its characteristics are described in Fig. 7, both in terms of impulse magnitude distribution of the fragmentation event and Gabbard diagram.

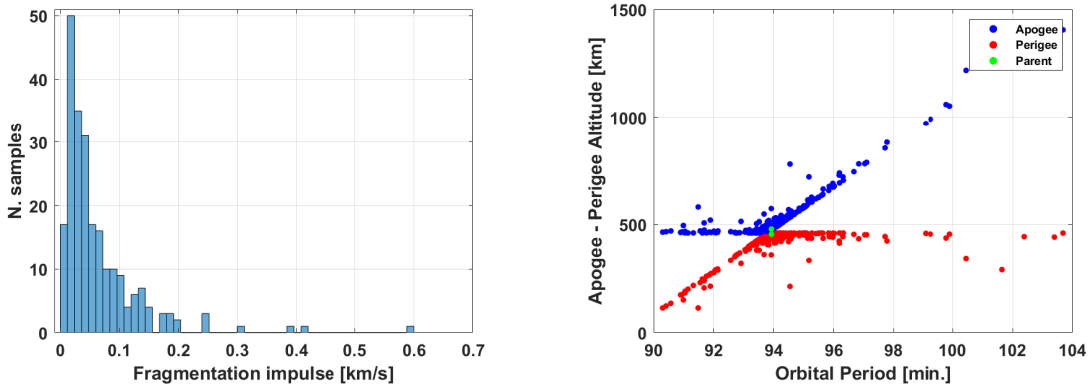

(a) Impulses magnitude distribution of the fragmentation event

(b) Gabbard diagram

Fig. 7: Fragmentation event

3. The obtained ephemerides, representing the fragments, are propagated until the epoch t_{obs}, when they are detected by a surveillance radar, and the orbital states $\left\{\boldsymbol{x}^{fg}, \boldsymbol{P}^{fg}\right\}$ are determined.

By this way all the inputs for the process described in Sec. 2 are obtained and FRED algorithm can be tested, considering an analysis time window ranging from 23:20 UTC of November 14th (epoch of the simulated last available ephemeris of the parent object) to 06:00 UTC of November 15th, retracing the fact that the COSMOS 1408 fragmentation alert was provided in the early morning (considering UTC coordinates). These two epochs correspond to t_{eph} and t_a introduced in Sec. 2. The t_{obs} is set 13 h after the event, as the method aims at reconstructing the fragmentation

epoch from a single fragment observation conducted in the hours right after the event.
Based on this data set, FRED is run on each fragment IOD result $\left\{\boldsymbol{x}^{fg}, \boldsymbol{P}^{fg}\right\}$ separately, considering N_s=1e+03 samples for the multinormal distribution.

3.1 Unperturbed scenario

First, the unperturbed scenario with no IOD orbital state error is tested to assess the theoretical characteristics of FRED algorithm. This simulation just associates a covariance $\boldsymbol{P}^{fg}$ (with standard deviations 2.6e-02 km and 7.0e-04 km/s, for position and velocity respectively, computed simulating an IOD with the method presented in [21]) to the nominal value $\boldsymbol{x}^{fg}$, that is the fragments propagated state vectors. The parent last available ephemeris $\boldsymbol{x}^{p}$ is the same used above to generate the fragmentation.
For a single fragment analysis, the result is considered successful if the difference between the epoch estimation and the correct value (t_{err}) is below a threshold quantity, which is set equal to 60 s in the analysis. As introduced in Sec. 2, FRED failures can be linked to either the MOID computation or to the distributions comparison performed through the EMD, and for this reason they are classified as follows:

- MOID failures - compliant: 1 min. $< t_{err}$ and $t_{err} < 3\sigma_t$. These are cases for which the fragment orbit orientation is so similar to the parent one that a slight change in the fragment orbit, occurring from fragment mean state to its samples, causes a remarkable variation in the MOID data computation. This leads to an erroneous estimation of the parent transit through the MOID, but the distribution is wide enough to include such an error. Therefore, the resulting epoch estimation is wrong, but statistically compliant.
- MOID failures - uncompliant: 1 min. $< t_{err}$ and $3\sigma_t < t_{err} < T^p/2$. In these cases, the erroneous estimation of the epoch is not mitigated by its uncertainty. The epoch estimation is wrong, but the error is smaller than the half of the parent orbital period, as the EMD-based statistical comparison did succeed.
- EMD failures: $t_{err} > T^p/2$. In these cases, the statistical comparison identified a not-correct cluster and, so, it returned the wrong result.

Fig. 8a shows, for each fragment analysed, the time error between the estimated and the correct fragmentation epochs. It is possible to notice that, over the 231 fragments analysed, 12 MOID failures occurred, out of which 11 are compliant and 1 is not. Then, 5 EMD failures are present, and they are cases for which the EMD metrics returns similar values across the candidates, among which the correct solution is always present. The results in percentage are summarised in Tab. 1. Fig. 8b shows the relationship between the time standard deviation associated to the estimated epoch and the magnitude of the impulse which generated the fragment. It is possible to notice that the compliant MOID failures are more likely to occur in those regions with small impulse magnitude and large time standard deviation. On the contrary, both uncompliant MOID and EMD failures generally present a much smaller time uncertainty (with one exception), but still with a not high fragmentation impulse.

Correct solutions	MOID failures - compliant	MOID failures - uncompliant [deg]	EMD failures
204 / 231	11 / 231	1 / 231	5 / 231
92.7 %	4.8 %	0.4 %	2.1 %

Table 1: Unperturbed scenario results.

To better assess the failures characteristics, the difference between parent and fragments orbital parameters is studied. From Fig. 9a and Fig. 9b it is possible to observe that the EMD failures regard cases in which the fragment orbit semi-major axis and the eccentricity is very close to the parent values. Indeed, in this situation, the two orbits have a similar period and shape, and, from a i-th periodicity to the following one, there is not a remarkable difference in the relative distance distribution $\boldsymbol{P}$ (the 3D MOID one $\boldsymbol{M}$ is always the same, being the scenario keplerian). This weakens the statistical comparison result, as the EMD is similar across multiple clusters, and the algorithm possibly converges to an erroneous solution. Instead, from Fig. 9c and Fig. 9d it is worth to notice that both compliant and uncompliant MOID failures regard cases in which fragment and parent inclination and right ascension of the ascending node are very close each other, as the similar orientation provokes problems in computing the MOID data.

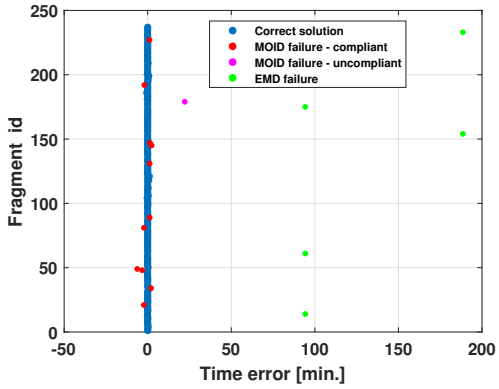

(a) Time error for each fragment of the data set. The fragments for which a failure occurs are highlighted according to the legend.

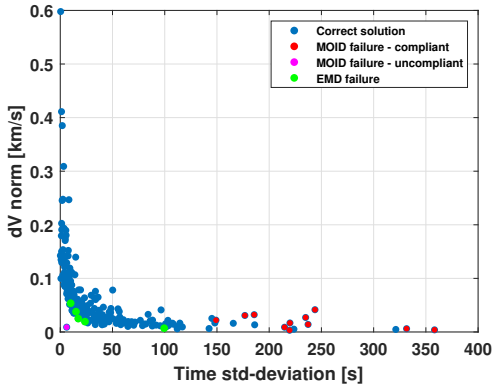

(b) Relationship between the impulse magnitude originating each fragment and the time standard deviation associate to the final result.

Fig. 8: Result of the numerical analysis on an unperturbed scenario with no orbital state error.

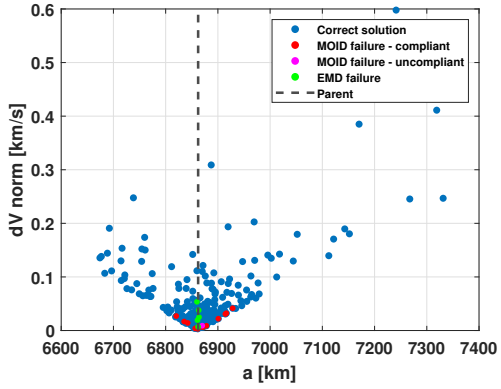

(a)

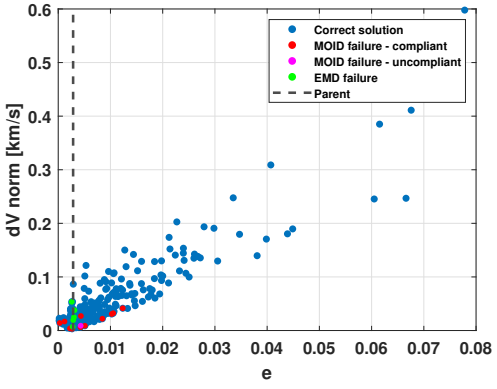

(b)

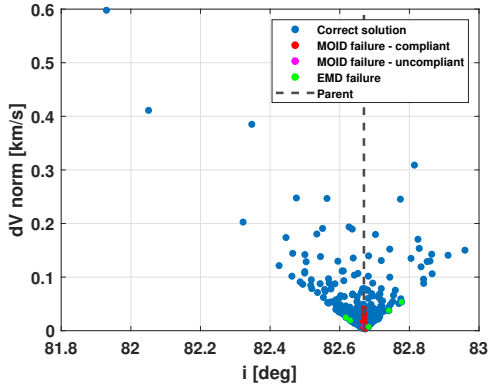

(c)

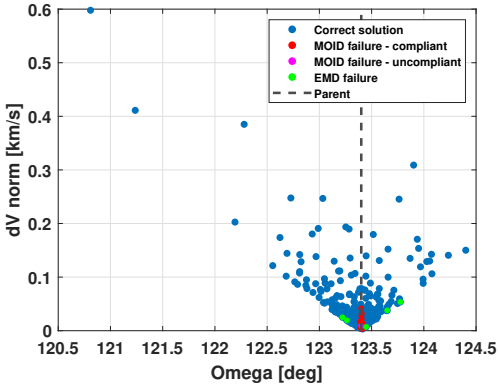

(d)

Fig. 9: Relationship between the impulse magnitude originating each fragment and the fragment semi-major axis (**a**), eccentricity (**e**), inclination (**i**) and right ascension of ascending node (**Omega**). The fragments for which a failure occurs are highlighted according to the legend, and the dashed line shows the parent orbital parameters.

3.2 Operational scenario

After having assessed FRED characteristics for an ideal unperturbed scenario in which the fragment mean state is exactly equal to the ground truth, a situation more similar to an operational situation has to be investigated, in which both the IOD process and the mismatching between the propagation model and the fragment actual trajectory is considered. Both of them introduce errors and, so, possibly affect the algorithm performance. The IOD process is simulated as run from measurements acquired by a surveillance radar, which, collecting both angular and slant range measurements with no need of pass prediction, allows to initially determine the orbit without other sensor contributions. Instead, for what concerns the propagation mismatching, SGP4 is used both to derive measurements and inside FRED, but with different values for B* [9] [10]: 6.9413e-05 to generate measurements and 3.47065e-05 (that is the half of the previous value) inside FRED. The former value is retrieved from the last available COSMOS 1408 TLE before the event.

As mentioned above, the European Space Surveillance and Tracking consortium [18] observed fragments generated by COSMOS 1408 fragmentation and the Bistatic Radar for LEO survey (BIRALES), an Italian bistatic radar system for space surveillance, was one of the most contributing sensors in the network [22]. For this reason, its characteristics are taken as reference.

The state vectors retrieved from the fragmentation are propagated until they intersect BIRALES receiver Field of View (FoV), and measurements are synthetically generated, which are azimuth, elevation and range. A Gaussian noise is then added, with standard deviations of 30 m for the range and 0.01 deg for Azimuth and Elevation, coherently with what presented in [22] about a real signal scenario. Since the method aims at estimating fragmentation epoch in a statistical way starting from a IOD result few hours after the break-up, the analysis focuses on the fragments intersecting BIRALES FoV within 1 day after the event, and this reduces the data set to 87 fragments, also accounting for those which reenter to the ground, due to the perturbations contribution which are absent in the keplerian scenario. These fragments are detected between 10.3 h and 12.4 h after the fragmentation.

Starting from the measurements, the IOD is performed according to the procedure described in [21], and the fragment orbital state $\left\{\boldsymbol{x}^{fg}, \boldsymbol{P}^{fg}\right\}$ at the observation epoch t_{obs} is obtained. Besides on the IOD algorithm used, the accuracy of such a state strongly depends on the observation geometry and the standard deviation considered in modelling measurements noise.

The results are reported in Tab. 2 and represented in Fig. 10a, with the same failures distinction as above: 3 MOID compliant failures, 2 MOID uncompliant failures and 12 EMD failures. The deterioration in EMD performance with respect to the analysis in Sec. 3.1 is motivated by the errors introduced both by the IOD result and the propagation model mismatching (different values of B*), which affects the EMD-based criterion. Nevertheless, the results are more appreciable than those reported in Tab 3 and represented in Fig. 10b, which are related to the fragmentation epoch estimation assessed through the relative distance metrics, that is performed by assessing the fragmentation epoch as the time of the minimum relative distance between the parent and the fragment mean state (both assumed as deterministic), propagated on the analysis time window. Through this latter metrics, only 16 solutions with $t_{err} < 60$ s are returned, and 65 failures with $t_{err} > 60$ s and $t_{err} < T^p/2$ occur, which cannot be indicated as compliant, as no uncertainty is associated to them. Finally, even if FRED returns more failures with $t_{err} > T^p/2$ than the relative distance metrics (12 against 6), the correct solution among the candidate clusters is always present.

Correct solutions	MOID failures - compliant	MOID failures - uncompliant [deg]	EMD failures
70 / 87	3 / 87	2 / 87	12 / 87
80.5 %	3.4 %	2.3 %	13.8 %

Table 2: Operational scenario: FRED results.

Correct solutions	1 minute $< t_{err} < T^p/2$	$t_{err} > T^p/2$
16 / 87 %	65 / 87	6 / 87
18.4 %	74.7 %	6.9 %

Table 3: Operational scenario: relative distance metrics results.

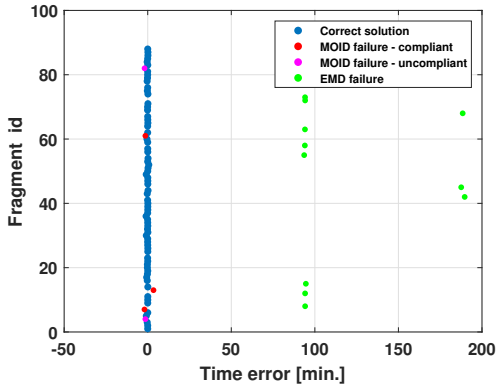

(a) Time error for each fragment of the data set by using FRED to estimate the fragmentation epoch. More EMD failures are present than in the Sec. 3.1 analysis.

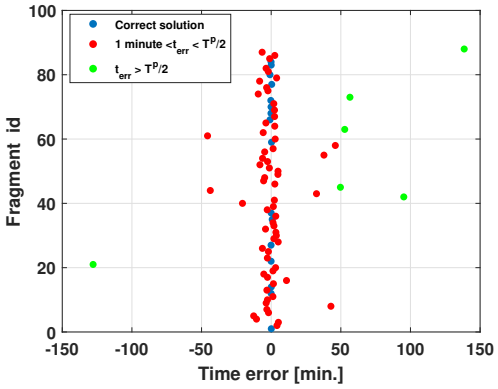

(b) Time error for each fragment of the data set by using the minimum relative distance between parent and fragment mean state to assess the fragmentation epoch.

Fig. 10: Fragmentation epoch estimation error. The fragments for which a failure occurs are highlighted according to the legend.

To conclude, the analysis proves that FRED algorithm represents a valid choice also in operational scenarios, where errors both due to the IOD process and the propagation model occur.

4. CONCLUSIONS

The paper described FRED algorithm, which detects the fragmentation epoch through a statistical method which starts from the IOD result of a single fragment and the last available parent ephemeris. The numerical simulations highlighted that the algorithm reliability decreases when the observed fragment orbit has either the period or the orbital plane similar to the parent object one. Nevertheless, FRED represents a valid choice in operational scenario simulation, as the dedicated analysis showed.
FRED algorithm allows to have a prompt estimation of the fragmentation epoch through a statistical model from the observation of a single fragment, with no need to wait until several fragments detection have been made. This prompt knowledge of the fragmentation epoch would allow to better plan following observations, and so to acquire more and more accurate orbit determination results immediately after the event, which possibly refine the fragmentation epoch estimation and, so, to plan further observations. By this way, a virtuous circle would be generated, leading to better monitor the fragment cloud evolution and to assess possible collisions.
In the future, FRED algorithm will be further validated through both synthetic and real data, by also accounting for the uncertainty of the parent object last available ephemeris. Finally, a possible application of FRED to the maneuvering detection problem is under study.

5. ACKNOWLEDGEMENT

The research activities described in this paper were performed within the European Commission Framework Programme H2020 and Copernicus “SST Space Surveillance and Tracking” contracts N. 952852 (2-3SST2018-20) and N. 299-G-GRO-COPE-19-11109 (1SST2018-20) and the support of the Italian Space Agency through the grant agreement n. 2020-6-HH.0 (Detriti Spaziali – Supporto alle attività IADC e SST 2019-2021).

[1] ESA. Space debris by the numbers. Available online at: `https://www.esa.int/Space_Safety/Space_Debris/Space_debris_by_the_numbers`, Last accessed August 18th, 2022.
[2] Inter-Agency Space Debris Coordination Committee. *Space Debris Mitigation Guidelines*, 2002.
[3] D. J. Kessler and B. G. Cour-Palais. Collision frequency of artificial satellites: The creation of a debris belt. *Journal of Geophysical Research*, page 2637–2646, 1978.

[4] Roxana L. Andrisan, Alina Ioniţă, Raúl Domínguez González, Noelia Sánchez Ortiz, Fernando Pina Caballero, and Holger Krag. Fragmentation event model and assessment tool (fremat) supporting on-orbit fragmentation analysis. In *7th European Conference on Space Debris*, 2016.

[5] S. Frey, C. Colombo, and S. Lemmens. Density based modelling and indication of break-up location and epoch from fragments using backwards propagation. In *5thEuropean Workshop on Space Debris Modelling and Remediation*, June 2018.

[6] L. Di Mare, S. Cicalò, A. Rossi, E. M. Alessi, and G. B. Valsecchi. In-Orbit Fragmentation Characterization and Parent Bodies Identification by Means of Orbital Distances. In *First International Orbital Debris Conference*, volume 2109 of *LPI Contributions*, page 6007, December 2019.

[7] M. Romano, A. Muciaccia, M. Trisolini, P. Di Lizia, C. Colombo, A. Di Cecco, and L. Salotti. Characterising in-orbit fragmentations with the puzzle software. In *8th International Conference on Astrodynamics Tools and Techniques (ICATT)*, 2021.

[8] F. R. Hoots, L. L. Crawford, and R. L. Roehrich. An analytic method to determine future close approaches between satellites. *Journal of Celestial Mechanics and Dynamical Astronomy*, 33(2):143–158, june 1984.

[9] Felix Roach Hoots and Roland Louis Roehrich. Spacetrack report no. 3 models for propagation of. 1988.

[10] David Vallado, Paul Crawford, Richard Hujsak, and T.S. Kelso. Revisiting spacetrack report 3: Rev. 08 2006.

[11] G. F. Gronchi. An algebraic method to compute the critical points of the distance function between two keplerian orbits. *Journal of Celestial Mechanics and Dynamical Astronomy*, 93(1):295–329, sept. 2005.

[12] S. Kotz, N. Balakrishnan, and N. L. Johnson. *Continuous Multivariate Distributions. Models and Applications*, volume Volume 1: Models and Applications. New York: John Wiley, 2nd edition edition, 2000.

[13] Martin Ester, Hans-Peter Kriegel, Jörg Sander, and Xiaowei Xu. A density-based algorithm for discovering clusters in large spatial databases with noise. In *Proceedings of the Second International Conference on Knowledge Discovery and Data Mining*, KDD'96, page 226–231. AAAI Press, 1996.

[14] David Vallado and Salvatore Alfano. Curvilinear coordinate transformations for relative motion. *Celestial Mechanics and Dynamical Astronomy*, 118, 02 2014.

[15] E. Levina and P. Bickel. The earth mover's distance is the mallows distance: some insights from statistics. In *Proceedings Eighth IEEE International Conference on Computer Vision. ICCV 2001*, volume 2, pages 251–256 vol.2, 2001.

[16] SciPy. Scipy documentation, 2022. Available online at: `https://docs.scipy.org/doc/scipy/`, Last accessed August 18th, 2022.

[17] EUSST. Cosmos 1408 fragmentation, 2021. Available online at: `https://www.eusst.eu/newsroom/eu-sst-confirms-fragmentation-cosmos-1408/`, Last accessed August 18th, 2022.

[18] EUSST. European space surveillance and tracking website, 2022. Available online at: `https://www.eusst.eu/`, Last accessed August 18th, 2022.

[19] Space-track. Space-track website, 2021. Available online at: `https://www.space-track.org/auth/login`, Last accessed August 18th, 2022.

[20] NASA. Proper implementation of the 1998 nasa breakup model. *Orbital Debris Quarterly News*, 15(4):4–5, 2011.

[21] J. Siminski. Techniques for assessing space object cataloguing performance during design of surveillance systems. In *in Proc. 6th International Conference on Astrodynamics Tools and Techniques (ICATT)*, 2016.

[22] M.F. Montaruli, L. Facchini, P. Di Lizia, M. Massari, G. Pupillo, G. Bianchi, and G. Naldi. Adaptive track estimation on a radar array system for space surveillance. *Acta Astronautica*, 2022.